



Cite this: DOI: 10.1039/d5mh02328a

Received 5th December 2025,
Accepted 20th April 2026

DOI: 10.1039/d5mh02328a

rsc.li/materials-horizons

First observation of dual electrical–optical percolation in metallic nanowire networks

Buyun Zheng,^a Sebastian Schumacher,^{ab} David Muñoz-Rojas,^a
Jean-Pierre Simonato^c and Daniel Bellet^{ib*}

Metallic nanowire (MNW) networks have attracted sustained interest due to their remarkable optical transparency, electrical conductivity, and mechanical flexibility, making them promising candidates for transparent electrodes in applications such as photovoltaics, touchscreens, electrochromic devices, transparent heaters, and low-emissivity coatings. Among MNWs, silver nanowires (AgNWs) have been the most extensively studied due to their well-controlled chemical synthesis and good stability. The strong link between the physical properties of MNW networks and their structural parameters—nanowire dimensions and network density—has been widely investigated, particularly regarding electrical percolation. We demonstrate in this article for the first time that in addition to the well-known electrical percolation, MNW networks also exhibit an optical percolation at a network density approximately six times higher. This optical percolation is revealed through the angular dependence of the infrared emissivity of AgNW networks with varying densities. When the network density exceeds an optical critical threshold, the AgNW networks display a distinctly metallic optical response. We further show, also for the first time, that AgNW networks above a critical density follow the Hagen–Rubens relation which was originally developed for metallic films. The ratio between critical network density for electrical and optical percolation was found to be independent of the diameter of the silver nanowire in the range of 58–112 nm. These findings provide new insights into the optical behaviour of MNW networks and offer valuable guidelines for optimizing their integration into industrial devices.

1. Introduction

In the field of functional nanomaterials, MNW networks—most commonly silver (AgNW), copper (CuNW), alloyed or core–shell

New concepts

Metallic nanowire (MNW) networks are widely used as transparent and flexible electrodes and their physical properties have been the subject of many investigations. The focus of research has been mainly on their optical and electrical properties as well as their integration into devices. In this work, we introduce two previously unrecognized concepts which extend the physical understanding of MNW networks and improve their controlled engineering. Firstly, we demonstrate that MNW films exhibit optical percolation, a distinct critical transition occurring at a network density far above the well-known electrical percolation threshold. Beyond this optical critical density, the networks switch from dielectric-like to metallic-like infrared angular emissivity, revealing that light interacts with the collective network rather than with individual nanowires. Secondly, we establish that dense AgNW networks follow a generalised Hagen–Rubens relation despite their strong microscopic inhomogeneity. This enables normal emissivity to be predicted directly from the sheet resistance. The discovery that the electrical and optical percolations as well as the threshold for Hagen–Rubens applicability occur at fixed network density ratios—independent of nanowire diameter—provides a simple, universal design rule for MNW-based devices. Our observations establish all three phenomena as fundamental nanowire network properties and open new pathways for designing low-emissivity coatings, infrared-responsive films, and other technologies that exploit percolation-driven optical transitions.

composites—have emerged as a leading materials platform for flexible, transparent, and stretchable electrodes.^{1–3} They can combine bulk-like electrical conductivity with optical transparency and mechanical compliance not attainable in continuous thin metal films or with transparent conductive oxides such as indium tin oxide (ITO).^{4,5} Their technological appeal spans many applications^{1,2} such as touchscreens, flexible displays, transparent heaters,⁶ photovoltaics, low-emissivity films⁷ and wearable electronics.

The defining feature of MNW networks is that electrical transport is carried by an interconnected, randomly ordered ensemble of conductive nanowires with high aspect ratio. Macroscopically measurable quantities such as the sheet resistance R_{sh} , optical transmittance T and mechanical robustness depend therefore not only on the intrinsic conductivity of the

^a Univ. Grenoble Alpes, CNRS, Grenoble INP, LMGP, Grenoble 38000, France.
E-mail: daniel.bellet@grenoble-inp.fr

^b Universidade Nova de Lisboa, NOVA School of Science and Technology, CENIMAT
| i3N, Caparica 2829-516, Portugal

^c Univ. Grenoble Alpes, CEA, LITEN, Grenoble 38000, France



metal but also strongly on the MNW geometry⁸ (nanowire length L_{NW} , diameter D_{NW} , curvature), network density and the junction resistance of nanowire–nanowire contacts^{9,10} which can be optimized by various welding methods.^{11,12} This geometric dependence means that randomly oriented MNW networks have a macroscopic conductivity which can be described by stick percolation theory: When the number of nanowires increases and makes the network denser, individual wires start to overlap and form conductive pathways. At the critical network density, the probability of finding continuous conduction pathways throughout the entire network approaches 50%.¹³ Near this threshold, the conductivity follows well-known scaling laws rather than simple linear mixing rules.¹⁴ The previously insulating layer becomes abruptly conductive¹⁵ and every new pathway increases the conductivity in a quantised step.¹⁶ Theoretical and experimental studies have identified MNW networks as inherently percolative systems.

In addition to percolation in a pure network of just one metallic phase, double percolation is known for the formation of two coupled percolating networks in multi-phase materials.¹⁷ It is a structural–topological phenomenon observed in such composites with multiple intertwined phases where each is distributed across the entire structure (co-continuous). One phase contains for instance an electrically or thermally conductive component (filler) within the other insulating host phase. The macroscopic conductivity of the materials depends on the ratio between these two phases. When the conductive phase reaches a critical proportion, its previously isolated components come into contact and form a completely continuous network. This formation corresponds to a sharp change in macroscopic conductivity from almost zero to positive values. Double percolation can occur for each phase at different ratios.^{18,19} The different thresholds are technologically significant because they permit ultra-low filler loadings while achieving high conductivity, which preserves mechanical performance, reduces cost and eases processing.²⁰ Recent studies have shown that morphology control (blend ratio, mixing sequence, crystallisation, and processing route including additive manufacturing) strongly affects the range of compositions that exhibit double percolation and the sharpness of the percolation transitions, making processing–structure control a primary design lever for next-generation multifunctional composites.²¹ This architecture dramatically lowers the effective filler loading required for macroscopic conduction and enables simultaneous tuning of electrical, thermal and mechanical properties, with important applications in sensors, electromagnetic interference (EMI) shielding, flexible conductors and printed/3D-printed functional components.^{21,22}

While double percolation in two-phase composites is well known, we report here a second percolation in angular emissivity of pure one-phase MNW networks. Both the electrical and emissivity properties vary between two states as a function of the network density. Our findings thereby introduce the new notion of dual percolation in which just one pure metallic phase exhibits two different percolative physical properties. Dual differs from double percolation in that it does not

necessarily require multiple phases but instead multiple percolation regimes. In the case of MNW networks, the conductivity exhibits electrical percolation and the angular emissivity optical percolation. Both can be described with the network density as their critical parameter.

Network density is key for characterising nanowire networks.¹³ The widely used areal mass density amd (often expressed in mg m^{-2}) accounts both for the numerical network density n (nanowires per μm^2) and nanowire geometry including length (L_{NW}) and diameter (D_{NW}). This makes it a convenient metric for measuring and comparing networks:

$$amd = n \cdot \rho_{\text{m}}^{\text{Ag}} \cdot \pi \cdot \frac{D_{\text{NW}}^2}{4} \cdot L_{\text{NW}} \quad (1)$$

where $\rho_{\text{m}}^{\text{Ag}}$ is bulk silver density of 10.49 g cm^{-3} .

The critical electrical $amd_{\text{c,el}}$ is the threshold at which electrical percolation is reached with a probability of 50%. Its value has been determined by Monte Carlo simulations^{14,23} for randomly oriented sticks as:

$$amd_{\text{c,el}} = \frac{5.64\pi}{4} \cdot \rho_{\text{m}}^{\text{Ag}} \cdot \frac{D_{\text{NW}}^2}{L_{\text{NW}}} \quad (2)$$

For dense AgNW networks with $amd > amd_{\text{c,el}}$ the sheet resistance across the network follows the power law:^{14,23}

$$R_{\text{sh}} = K \cdot (amd - amd_{\text{c,el}})^{-4/3} \quad (3)$$

assuming that instrumental contact resistance can be ignored.

Classical percolation models have evolved to account for real nanowire systems. Langley *et al.* showed that length polydispersity lowers $amd_{\text{c,el}}$, while nanowire curvature causes only a modest increase.¹³ Later studies, including the one by Lee *et al.*,²⁴ confirmed that curvature can indeed raise the $amd_{\text{c,el}}$, especially in solution-processed networks where nanowires bend easily. Schneider *et al.* introduced a “two-junction model” demonstrating that junction resistance must approximate $<10 \Omega$ to maximize conductivity.²⁵ Forró *et al.* developed a closed-form analytical model linking network density to effective conductivity, enabling optimization without heavy simulation.²⁶

Many other physical network properties have been investigated such as the optical transmittance,¹⁴ the haziness (ratio between diffuse and total transmission),²⁷ the mechanical flexibility,⁴ and infrared (IR) emissivity.^{28,29} The dependence of those properties on L_{NW} , D_{NW} , amd , and post-deposition treatment has also been investigated. However, so far there has been no in-depth study linking optical and electrical properties directly. We report in this article strong experimental correlation between electrical conductivity and IR emissivity of MNW networks.

A correlation between optical and electrical properties has been known for the normal emissivity and sheet resistance of thin metal films as expressed in the Hagen–Rubens relation.³⁰ It is the classic low-frequency asymptote linking a metal’s good reflectivity to its direct current conductivity. In the far-infrared (FIR) limit where the angular probing frequency ω is much smaller than the charge-carrier scattering rate ($\omega \ll \tau^{-1}$) and interband contributions are negligible, the normal-incidence



reflectivity $r(\omega)$ of a bulk, highly conducting metal can be written as an expansion of the Fresnel result.^{30,31} To leading order, one obtains the familiar Hagen–Rubens form:

$$r(\omega) \approx 1 - 2\sqrt{\frac{2\varepsilon_0\omega}{\sigma_{\text{DC}}}} \quad (4)$$

where ε_0 is the vacuum permittivity and σ_{DC} the frequency-independent direct current conductivity. This square root frequency dependence follows directly from combining the Drude description of the metal dielectric function with the Fresnel reflection coefficients in the limit of large complex refractive index.

Because it connects an easily measurable optical quantity (low- ω reflectivity) to the direct current conductivity, the Hagen–Rubens relation is widely used in IR spectroscopy:^{32–34} (i) as the low-frequency extrapolation needed for Kramers–Kronig transforms of reflectivity data, (ii) to estimate spectral emissivity from resistivity for thermal/energy-management applications, and (iii) as a simple check of Drude-like metallic behaviour in materials. Practical applications and experimental examples include infrared emissivity/low- ϵ coatings, electron correlation and superconducting materials studies, and thin-film thermal radiation engineering.

For metallic thin films, eqn (4) can be adapted by introducing the normal infrared emissivity ϵ_{\perp} . It is the ratio of the IR emission of a given material relative to that of a perfect blackbody. A brief discussion of the derivation of the Hagen–Rubens relation in eqn (4) can be found in the book by Born and Wolf:³⁵

$$\epsilon_{\perp}(\omega) = 2\sqrt{2\varepsilon_0\omega\rho_{\text{DC}}} \quad (5)$$

where ϵ_{\perp} is the normal IR spectral emissivity and ρ_{DC} the electrical resistivity of the thin metallic film.³⁶

For MNW networks, the electrical conductivity is not an intuitive physical notion since such a network cannot be treated like a homogenous thin film. However, one can translate the relation expressed in eqn (5) by introducing the sheet resistance R_{sh} which is proportional to the studied material electrical resistivity:

$$\epsilon_{\perp} = K_{\omega}\sqrt{R_{\text{sh}}} \quad (6)$$

where K_{ω} is a constant for a given angular frequency ω . Eqn (6) is then an adapted expression of the Hagen–Rubens relation to assess whether it still holds valid for MNW networks, since one can measure both the normal emissivity (*i.e.* emissivity measured along the direction perpendicular to the sample surface) and the sheet resistance for various network densities.

Optical properties are investigated in this article through the angular dependence of network emissivity. It is known that dielectric materials (such as oxides) generally exhibit large IR emissivity (>0.8) which decreases at high inclinations relative to the sample normal. In contrast, the IR emissivity of metals is very low (<0.1) but tends to increase with increasing angle.³⁷

We demonstrate experimentally in this article that AgNW networks behave optically as dielectrics when they are sparse, but as metals above a critical optical density which is much

larger than the electrical threshold. Therefore, we show for the first time that metallic nanowire networks do exhibit dual percolation, between electrical and optical properties. We also demonstrate the existence of an optical threshold thanks to another approach, by comparing the normal infrared emissivity of AgNW networks and their sheet resistance: the Hagen–Rubens relation is actually valid for AgNW networks denser than a critical density which is also much larger than the electrical threshold. We also assess the influence of the AgNW diameters on this dual percolation.

2. Materials and methods

2.1. Silver nanowires

AgNW suspensions in isopropanol were purchased from ACS Material LLC (Pasadena, USA) and diluted to 0.1–1 g L⁻¹ before use. Four types of AgNW with different characteristic dimensions were used in this study, as detailed in Table 1. The lengths and diameters of nanowires were measured from scanning electron microscopy (SEM) images using ImageJ software, with more than 100 nanowires randomly analysed for each sample to ensure representative results. Alkaline earth borosilicate glass (Corning 1737, Corning Inc., USA) was used as substrate throughout this study, each with sizes of 25 × 25 × 1.1 mm³. Prior to deposition, the substrates were cleaned ultrasonically in isopropanol and de-ionised water for 15 min each and then dried with nitrogen gas.

2.2. Network deposition and annealing

AgNW networks were deposited on the substrates using a home-made spray-coating system in air.³⁸ The spray coating head was an Infinity CRplus Two in One airbrush (Harder & Steenbeck, Norderstedt, Germany) equipped with a 0.4 mm fine line nozzle. Nitrogen was used as carrier gas at a pressure of 1.4 bar. The spray pattern followed a zigzag trajectory with a scanning speed of 50 mm s⁻¹ orthogonally at a distance of 76 mm. During deposition, the substrates were always heated to 110 °C for immediate solvent evaporation to ensure homogeneous deposition and avoid the formation of “coffee rings”.³⁹ The density of the networks was controlled by varying the number of spray cycles. Spraying margins of 15 mm ensured a homogeneous deposition without deficiency at the edges. The resulting nanowire networks are completely random without preferential alignment. All samples were then annealed at 200 °C in air for 1 hour to weld overlapping nanowires into each other and achieve minimal junction resistance.¹¹ The AgNW morphology during the annealing did not change as can be seen in Fig. S1. Notably, the impact of the thermal

Table 1 Silver nanowire dimensions measured by SEM

	Ag58	Ag73	Ag95	Ag112
D_{NW} (nm)	58 ± 11	73 ± 13	95 ± 18	112 ± 21
L_{NW} (μm)	25.3 ± 15.6	19.5 ± 11.0	19.7 ± 9.8	20.1 ± 10.6



annealing on infrared emissivity and optical transmittance of AgNW network is negligible (see Fig. S3a and b, respectively).

2.3. Characterisation of AgNW networks

2.3.1. Network areal mass density (amd). The diameter of the AgNW was first determined from SEM images using Fiji/ImageJ. For each AgNW batch, over 200 individual nanowires were measured to ensure statistical reliability, with the corresponding size distributions provided in Fig. S4. The *amd* was used in this study to quantify the density of AgNW networks. It was determined from SEM images using the “ridge detection” plugin^{40,41} in Fiji/ImageJ⁴² which traces all individual nanowires to extract the areal line density ($n \cdot L_{\text{NW}}$). By incorporating the measured mean diameter, the *amd* was computed according to eqn (1). For each sample, SEM images with different magnifications were selected depending on the nanowire density, ensuring accurate measurement while maintaining clear visualization of the nanowire network. The reported *amd* values were obtained by averaging the results from five SEM images taken from randomly selected areas.

2.3.2. IR emissivity. The samples were heated to 114 °C on a heating plate and a FLIR T335 (30 Hz) IR camera with a focal-plane array (FPA) uncooled microbolometer detector measured the apparent sample temperature on the top side. The declared accuracy amounts to ± 2 °C for a detection range of 7.5–13 μm . The measurement was automatically corrected for a measuring distance of 500 mm. The apparent temperature T_{app} was then converted into the equivalent infrared radiance (L) using the following calibration from Riou *et al.*:⁴³

$$L(T_{\text{app}}) = 0.0108 \cdot T_{\text{app}}^2 + 1.7054 \cdot T_{\text{app}} + 89.504 \quad (7)$$

A soot blackbody ($\epsilon \approx 0.98$) and a silver thin film reflector ($\epsilon \approx 0.03$) from physical vapor deposition were taken as reference standards for nearly complete and inexistent emissivity, respectively, to convert the radiance into emissivity:

$$\epsilon = \frac{L_{\text{sample}} - L_{\text{reflector}}}{L_{\text{blackbody}} - L_{\text{reflector}}} \quad (8)$$

For angular emissivity measurements the IR camera was directed at the sample from different angles θ while maintaining a constant distance.

2.3.3. Sheet resistance. The sheet resistance R_{sh} of the AgNW networks was measured using a four-point probe system (Lucas Labs Pro4). All four contacts were placed 7 mm apart. The electrical variables were quantified on a Keithley 2500 multimeter. Every network was measured at five different spots and the results averaged.

2.3.4. Optical transmittance. Optical transmittance T was obtained on a PerkinElmer Lambda 950 spectrophotometer in the range of 250–2500 nm using tungsten and deuterium lamps and an integrating sphere detector. Data-points were gathered at wavelength intervals of 5 nm. The sum of direct and diffuse radiation was measured with a white reflector plate.

2.3.5. Scanning electron microscopy. Scanning electron microscopy (SEM) was performed on a FEG-SEM Zeiss Gemini 300 (Carl Zeiss Microscopy GmbH, Oberkochen, Germany) with field-emission gun at 5 keV accelerating voltage. The aperture was kept at 30 μm at all times. Material contrast was recorded on an InLens energy-selective back-scattering electron detector. To avoid electric charging during the measurement, all samples were coated with a 3 nm layer of carbon using a Safematic CCU-010 high vacuum glow discharge coater.

3. Results and discussion

The results and associated discussion below are organized as follows: In the first part, we consider one AgNW dimension (Ag73) and report the influence of network density on the electrical sheet resistance and IR emissivity. Part 3.2 explores the angular dependence of emissivity still for Ag73 at different network densities. A dual electrical and optical percolation is clearly demonstrated. We also assess the validity of the Hagen–Rubens relation between sheet resistance and normal emissivity depending on AgNW network density. Part 3.3 shows the evolution of these properties for different AgNW dimensions (detailed in Table 1).

3.1. AgNW network properties for varying *amd*

Our observations of electrical percolation and optical transmittance confirm the previously reported relationships with the network density. Representative SEM images from our series of Ag73 samples with increasing *amd* = 4.3, 19.2, and 79.8 mg m^{-2} are shown in Fig. 1 on top. In the bottom row the physical network properties are outlined. Fig. 1a portrays sheet resistance after thermal annealing and exhibits clearly percolative behaviour at the critical $amd_{\text{c,el}}$ after which conductive pathways enable finite resistances. The sheet resistance quickly assumes single-digit values with a convergence to $\approx 1.1 \Omega \text{sq}^{-1}$. The observed $amd_{\text{c,el}} = 15.7 \text{ mg m}^{-2}$ is very close to the theoretical value of 12.6 mg m^{-2} according to eqn (2) and near the central SEM image of Fig. 1 where one can spot the handful of conductive pathways.

As long as the radiation frequency does not surpass the material-specific plasma frequency, the reflection by a metallic film depends mainly on its surface coverage, which is linearly proportional to the *amd* in the studied range. Optical transmissivity therefore decreases linearly with network density. The experimental transmittance data and the regression in Fig. 1b are in perfect accordance with their approximated formula by Lagrange *et al.*¹⁴ which validates both our transmission measurement itself and the *amd* determination. The normal infrared emissivity, also shown in Fig. 1b, exhibits a decrease when the network becomes denser, too. This can be understood in analogy to visible radiation. Additionally, metal nanowires can also absorb and re-emit infrared wavelengths. This simultaneous occurrence of different mechanisms renders the decrease non-linear. The exact dependence is beyond the scope of this study.



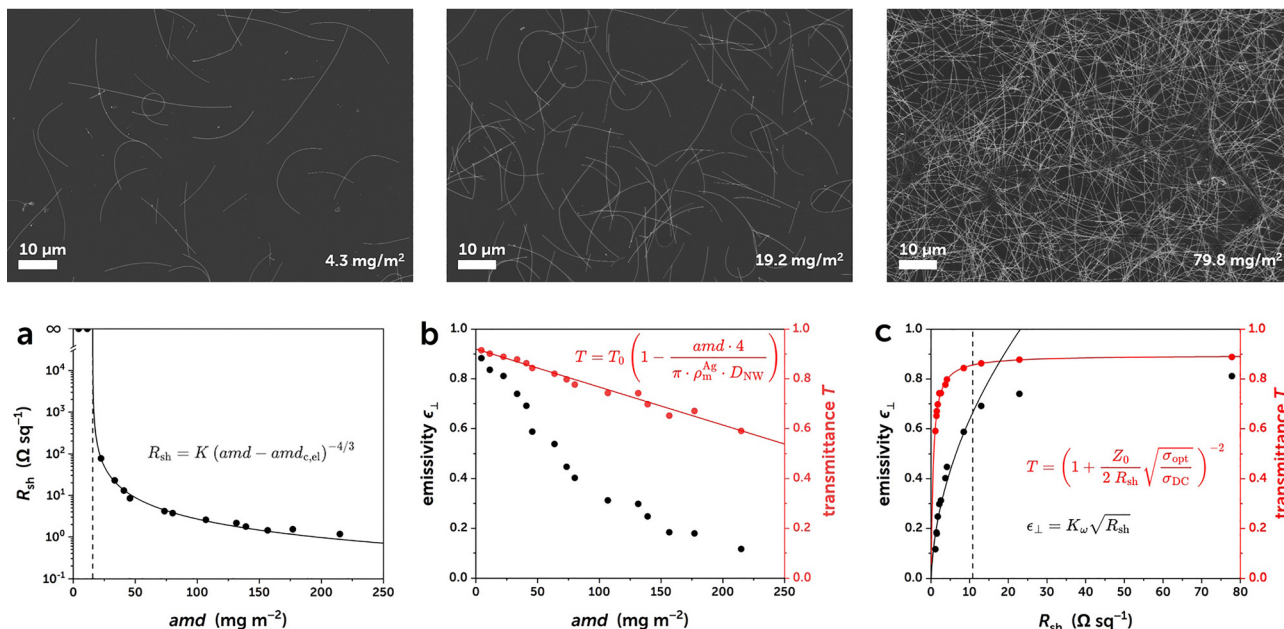


Fig. 1 Top row: SEM images of Ag73 nanowire networks at three different amd (value on bottom right). The central image is very close to the electrical percolation. Bottom row: (a) sheet resistance R_{sh} and black fit according to eqn (3), (b) normal emissivity ϵ_{\perp} in red and visible transmittance T in black with linear regression and formula for different areal mass densities amd of Ag73, (c) normal emissivity in black fitted to Hagen–Rubens eqn (6) and visible transmittance T in red against sheet resistance with respective formulae. All fits in (c) have an additional offset to compensate for the glass substrate. Transmittance is measured at 550 nm close to the maximum human photopic efficacy.

Fig. 1c applies the Hagen–Rubens theory to nanowire networks. Even though this theory was only developed for homogeneous thin films, we found dense networks to follow the same power law. The adapted eqn (6) with an offset fits well for low sheet resistances $R_{sh} < 10.7 \Omega \text{ sq}^{-1}$ or $amd > 50 \text{ mg m}^{-2}$ for medium to dense networks which are of interest to electric applications. In this regime, the well-percolating networks form sufficiently close connections to enable electron–light interactions similar to the bulk metal. The minimal amd beyond which this theory holds true will be denoted as $amd_{min,HR}$. The emissivity of sparser networks with higher sheet resistances is overestimated because homogeneous films of the same value would be vanishingly thin and easily traversed by irradiation without much interaction. Since the nanowire dimensions are equal for all resistances and only the gap sizes in the network vary, the Hagen–Rubens relation can only be applied to a limited extent. Nevertheless, it provides a very useful connection for the design of low-emissivity coatings for heat shielding. This relation enables optimal adjustment of the density of metal nanowire networks to achieve targeted emissivity properties.

3.2. Angular emissivity for varying amd

The angular IR emissivity differs for dielectrics and metals according to Fresnel's equations of s - and p -polarised radiation. It remains fairly constant at low and moderate angles for insulators because the increase in s -polarised reflectivity is compensated by a decrease of the p -polarised component. At high angles, both decrease rapidly until they reach zero at grazing incidence. In contrast, electrical conductors have a

much lower overall emissivity which increases progressively towards high angles. This trend results from high, angle-insensitive reflectivity for both polarisations. They undergo a synchronous drop at grazing incident (which would be 90°).^{44,45} In the case of AgNW networks, we observe a progression from sparse networks acting optically like an insulator to dense networks with an angular emissivity like conductors.

Fig. 2a shows a sketch of the angular measuring technique and two infrared thermal images taken at $\theta = 5^\circ$ and 80° inclination from the surface normal. Bright colours represent high apparent temperatures caused by high emissivity and dark colours low temperatures for low emissivity. The bright soot blackbody and the dark silver reflector serving as reference materials are in the top row. When comparing both angles, the mostly electrically insulating soot appears darker at 80° whereas the metallic silver film reflector is slightly lighter. They exemplify the different trends in angular emissivity for insulators and conductors and serve as calibrators. The three sample squares in the lower row are AgNW networks with increasing density from left to right. The colour becoming darker indicates a reduction in emissivity. When comparing the colours at 5° and 80° , the first sample darkens visibly, the second remains at a similar darkness whereas the third lightens up considerably. The differences in emissivity trends are shown in Fig. 2b for twelve different AgNW network densities at ten angles with $5^\circ \leq \theta \leq 80^\circ$. The sparse networks in yellow behave like dielectrics and the dense ones in black like metals. In between are two AgNW networks in grey whose behaviour cannot be solely classified as dielectric or metallic.



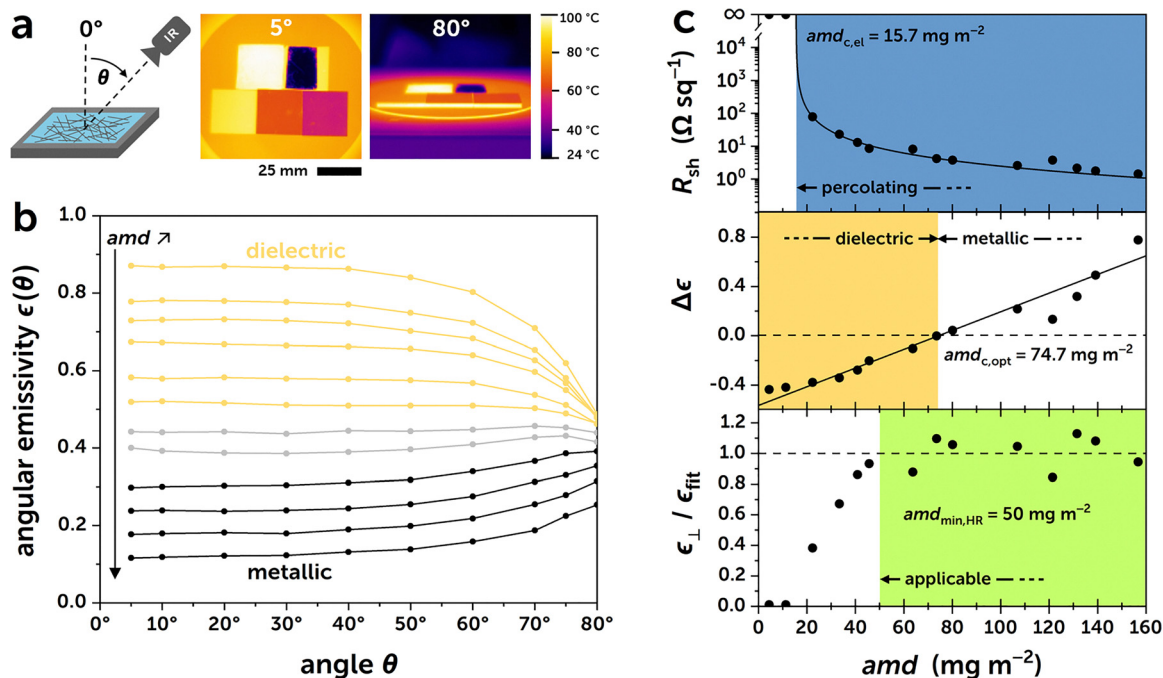


Fig. 2 (a) Photometry measurement setup for IR emissivity and two thermal images at 5° and 80° inclinations, (b) angular emissivity $\epsilon(\theta)$ for Ag73 network with dielectric-like curve form for low amd and metallic behaviour for high amd , (c) electrical and optical percolations, and Hagen–Rubens applicability as fitting accuracy.

To quantify this behaviour, we calculated the relative difference of emissivity close to orthogonal and tangential angles as:

$$\Delta\epsilon = \frac{\epsilon(80^\circ) - \epsilon(5^\circ)}{\epsilon(5^\circ)} \quad (9)$$

Dielectrics have $\Delta\epsilon < 0$ and metals have $\Delta\epsilon > 0$. Between these two regimes is what we call optical percolation at $\Delta\epsilon = 0$. While the $\Delta\epsilon$ value slightly depends on the selected angles for the calculation, the corresponding density for the transition from negative to positive $\Delta\epsilon = 0$ does not. This is shown in Fig. S5 where $\Delta\epsilon$ was calculated using different pairs of angles (5°–80°, 5°–75° and 5°–70°) and the corresponding critical amd when $\Delta\epsilon$ crosses zero remains similar.

Given the high absorptivity of glass in the infrared band (typically 7.5–13 μm), it is pertinent to ascertain whether the observed data in Fig. 2b are influenced by the nature of the substrate utilised. Therefore, a series of comparative experiments have been conducted on a silicon substrate as opposed to a glass substrate. The Si wafers were etched with 1% hydrofluoric acid to remove the silicon dioxide layer, after which the AgNW deposition and angular emissivity measurements were immediately performed. The observations made on both glass and silicon substrates exhibited the same angular emissivity trend (Fig. S6), indicating that the nature of the substrate used was not a determining factor.

Fig. 2c shows the electrical percolation on top and the optical percolation in the middle by plotting, respectively, the dependence of the sheet resistance and $\Delta\epsilon$ with AgNW network density. The critical electrical $amd_{c,el}$ is clearly much lower than

the critical optical $amd_{c,opt}$. The evolution of the relative difference of angular emissivity $\Delta\epsilon$ depends linearly on the amd which supports our assumption that this effect is indeed based on network density. We thus observe dual electrical and optical percolation for metal nanowire networks at different critical densities and different percolation behaviours. To the best of our knowledge, this is the first time that dual percolation is observed for a monomaterial. Importantly, the measured emissivity does not change before and after thermal annealing of the nanowire junctions (Fig. S3a). This observation proves that the macroscopic electrical conductivity is not directly correlated with the emissivity. As a consequence, the observed optical percolation is independent of the actual macroscopic conductance. It does, however, depend on the network density which can be related to the annealed network conductance.

The lower diagram of Fig. 2c shows the normal emissivity relative to the fitted Hagen–Rubens power law in eqn (6). One can easily compare the applicability range of this relation with the amd instead of the sheet resistance as abscissa. Nanowire networks with $amd_{min,HR} > 50 \text{ mg m}^{-2}$ give good agreement while sparser ones are out of bounds. Such results can be physically understood since denser AgNW networks behave more like metals and are then more prone to satisfy the Hagen–Rubens relation, which was demonstrated for homogeneous metal thin films but at a larger IR wavelength.³¹ The network-density threshold, $amd_{min,HR}$, above which the Hagen–Rubens relation accurately describes AgNW networks can be regarded as a critical network density.

All three critical amd values are different from each other and characterise three separate regimes for metal nanowire



network properties. Electrical and optical percolation are two phenomena with completely physically valid properties. Because these properties result from the nanowire density of the network, they are referred to as percolation. The applicability of the Hagen–Rubens relation, on the other hand, is a description analogous to thin films with limited validity for nanowire networks. Its prediction is incorrect below the minimum amd and therefore does not count as a third percolation. However, because applicability also depends on network density, all three regimes are herein discussed together.

3.3. Influence of AgNW dimensions on dual percolation

We studied the dual percolation behaviour of AgNW with average diameters of 58, 73, 95, and 112 nm, respectively. While the former has an average length of 25 μm , all others are approximately 20 μm long (see Table 1).

Fig. 3 outlines the evolutions of sheet resistance, angular emissivity difference, and Hagen–Rubens fit for all nanowire diameters. The trends are overall very similar—only the three respective critical network densities increase with higher diameters. This increase stems directly from the definition of amd which depends linearly on the mass of the network. Wider nanowire diameters weigh more for the same number of nanowires and the amd is thus higher for the same numerical network density n . The linear fit curves for the relative difference of angular emissivity are steeper for smaller nanowire diameters and the negative offset is larger. The steepness reflects the amd as choice of density measure. Since a cylindrical nanowire with big volume has a smaller side area than two smaller cylinders of equal total mass, the surface coverage increases quicker for thinner diameters at the same amd values and the emissivity change is more pronounced.

Table 2 summarises the critical amd and n values for both percolation regimes and the Hagen–Rubens applicability. While the critical amd continuously increases for higher nanowire diameters, the numerical network density remains

strikingly constant—albeit with significant deviation in some instances.

The densities, averaged over the four AgNW diameters, for the three regimes are $\langle n_{c,el} \rangle = 14\,800\text{ mm}^{-2}$, $\langle n_{\text{min,HR}} \rangle = 50\,200\text{ mm}^{-2}$, and $\langle n_{c,opt} \rangle = 84\,100\text{ mm}^{-2}$. These values stand at a ratio of 1:3.4:5.7. As shown in Fig. 4f, the observed $n_{c,el}$ and $amd_{c,el}$ is in good agreement with the theoretically predicted value from Li *et al.*⁴⁶ and the derived eqn (2), respectively. The values differ by less than 25% because not all AgNW really contribute to electrical conduction since small junctions between AgNW have been degraded during the thermal annealing while larger junctions are not yet welded. The consistency of the critical numerical network densities and the geometrically induced increase in the respective amd values indicate an underlying dependence on the surface coverage sc . All three density measures are approximately proportional to each other:

$$n \sim \frac{amd}{D_{\text{NW}}^2} \sim \frac{sc}{D_{\text{NW}}} \quad (10)$$

The surface coverage is very easily detected from SEM images. However, low object contrast, charging effects, and leftover nanoparticles can distort the measurement and cause greater variance than the more accurate nanowire detection for amd . The rough critical values are $\langle sc_{c,el} \rangle = 0.04$, $\langle sc_{\text{min,HR}} \rangle = 0.12$, and $\langle sc_{c,opt} \rangle = 0.23$. While sc , amd , and n are theoretically equivalent for physical analysis, one should preferentially use the latter two since they can be determined more accurately.

To understand the optical percolation further, we extended our investigation on the relation between the angular emissivity and the surface coverage by measuring the gap sizes within our nanowire networks from the SEM images. There are three commonly used measures for the size of irregular particles:⁴⁷ Feret diameter, and the equivalent circular diameter (ECD) based on either area or perimeter. The Feret diameter is usually only given as the maximum or minimum width of each particle.

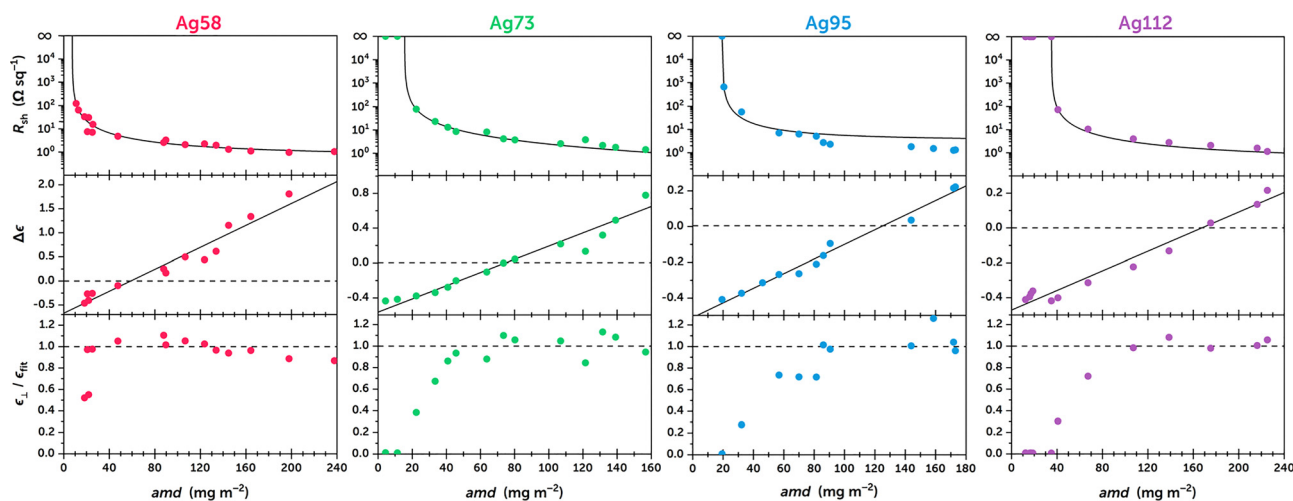


Fig. 3 Sheet resistance R_{sh} , relative difference of angular emissivity $\Delta\epsilon$, and relative accordance between normal emissivity ϵ_{\perp} and data fit according Hagen–Rubens eqn (6) against amd for AgNW with average diameters of 58, 73, 95, and 112 nm, respectively. The average length for Ag58 is 25 μm , all others are approximately 20 μm .



Table 2 Measured critical network densities amd and n for electrical percolation, optical percolation, and Hagen–Rubens applicability

	$amd_{c,el}$ (mg m ⁻²)	$n_{c,el}$ (10 ⁴ mm ⁻²)	$amd_{min,HR}$ (mg m ⁻²)	$n_{min,HR}$ (10 ⁴ mm ⁻²)	$amd_{c,opt}$ (mg m ⁻²)	$n_{c,opt}$ (10 ⁴ mm ⁻²)
Ag58	7.5	1.06	25	3.55	58.4	8.28
Ag73	15.7	1.85	50	5.89	74.7	8.80
Ag95	19.3	1.32	80	5.48	125	8.56
Ag112	34.9	1.67	107	5.15	167	7.99

However, network gaps are convex polygons with strong anisotropy (*i.e.*, highly irregular) and would not be adequately characterised with just two extreme spans. Calculating its average for all spatial directions is not straightforward. We decided to use the *ECD* which takes the area of the polygon and calculates the diameter of a circle with the same area:

$$ECD = 2\sqrt{\frac{\text{area}}{\pi}} \quad (11)$$

This method is extensively used for comparing particle sizes and easily implemented.⁴⁸ Its accuracy is obviously best for circular particles. Since our polygons fulfil that requirement only to a certain extent, the following results based on the *ECD* should only serve as a rough estimate. In addition, the random network has a wide distribution of gap sizes and only the mean values were considered.

Fig. 4a exhibits the relative difference of angular emissivity $\Delta\epsilon$ against different amd , along with crosshair cursors associated to the optical percolation for all four AgNW diameters at

$\Delta\epsilon = 0$. For each fabricated AgNW network we measured the gap sizes and obtained distributions like the one in Fig. 4b. The striking asymmetry with a far higher number of small gaps and fewer large ones makes a fitting choice of statistical measure rather difficult. We decided to take the mean gap size for each network and calculated the diameter of a perfect circle with the same area according to eqn (11). This afforded the *ECD* which is shown in Fig. 4c for each network sample. As expected, the *ECD* decreases rapidly with growing amd . The gaps shrink quickly when networks become denser. Black crosshair cursors indicate again the critical optical density. It appears that the optical percolation always takes place when an $ECD \approx 1.51 \pm 0.07 \mu\text{m}$ with a corresponding mean gap area of $1.79 \mu\text{m}^2$ is reached. This correlation proves the existence of a common critical gap size, at least in the studied AgNW diameters range of 58–112 nm. Even though one might expect special interactions when the gap size approaches the radiation wavelength, this average width is far smaller than the measured wavelength range of 7.5–13 μm . And the pronounced positive skewness of the gap distributions at the $amd_{c,opt}$ means that the most

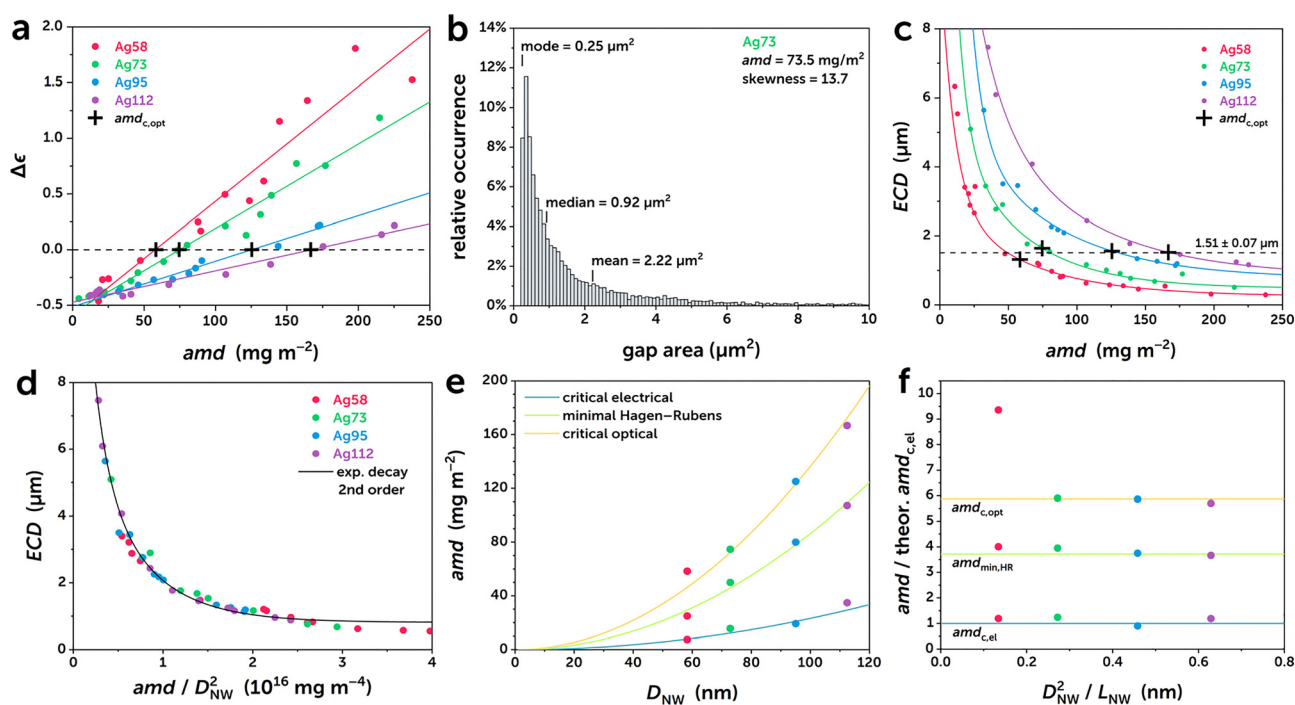


Fig. 4 (a) Relative difference of angular emissivity $\Delta\epsilon$ against different amd , (b) gap size distribution for Ag73 near the optical percolation, (c) corresponding mean equivalent circular diameter (*ECD*) for different network densities and nanowire diameters D_{NW} . The optical percolation is indicated by black crosshair cursors. (d) Evolution of *ECD* gap size corrected for diameter, (e) theoretical $amd_{c,el}$ according to eqn (2) and fitted multiples for $amd_{min,HR}$ and $amd_{c,opt}$ for different diameters, and (f) ratio of fitted multiples and theoretical critical electrical density.



frequently occurring ECD ($\approx 11\%$) is only about one third of the mean value used for further discussions. These results underline again the mainly qualitative character of the ECD analysis.

This observation corresponds to a sub-wavelength condition where the feature size of about $1.5\ \mu\text{m}$ is much smaller than the irradiation wavelength at $7.5\text{--}13\ \mu\text{m}$. Rather than with geometric optics, the optical response should be understood in an effective medium description. In this long-wavelength regime, emissivity is primarily controlled by the emergence of a continuous conductive network consistent with the transition towards metallic behaviour (Hagen–Rubens). Electromagnetic fields probe the network through its effective conductivity rather than individual gaps. One can therefore expect the optical percolation threshold to take place at shorter infrared wavelengths even though its spectral signature may evolve as the structural scale approaches the wavelength limit. The gap size as structural descriptor should not be interpreted as a geometrical optical aperture in the sense of diffraction, but rather as an effective structural correlation length governing the transition from disconnected to electromagnetically coherent conductive pathways. The physical interpretation of this phenomenon will certainly be the subject of future experimental and modelling work.

When correcting the ECD for the nanowire diameter (*i.e.* by plotting ECD against amd/D_{NW}^2) in Fig. 4d, all measured gap sizes correspond to the same network density. The exponential fitting curve yields excellent accuracy and enables the gap size to be predicted directly from the amd and AgNW diameter, or indirectly from the numerical network density n .

Fig. 4e compares the critical electrical, optical, and the minimal amd for Hagen–Rubens applicability for all four AgNW diameters. The critical network density from eqn (2) is taken as a trend line and multiples of it are fitted to the two other regimes. The fits capture the data very well. The ratio between the fitting curves is $1:3.7:5.9$ as shown in Fig. 4f. The close agreement between this ratio and the ratio of average numerical critical network densities n validates the dependency on network density independent of nanowire diameter. Only the $amd_{\text{c,opt}}$ for Ag58 is not well captured which might hint at non-geometric influences coming into play for very small nanowire diameters. While the lengths appear much larger compared to the value of the ECD so that we can reasonably discard it as the reason for this observation, metallic nanowires with smaller diameter exhibit stronger and more confined surface plasmon effects. This is due to enhanced field confinement, geometric scaling of plasmon modes, larger surface-to-volume ratio, and size-dependent dielectric response.

The transition from dielectric-like to metal-like optical behaviour in AgNW networks can be interpreted either as near-field coupling with plasmonic hybridization or in the framework of localisation physics.

The first option considers a collective electronic phenomenon arising from the interplay between electrical percolation, carrier delocalization, and electromagnetic coupling. At low densities, the network is composed of isolated or weakly connected nanowires and charge carriers remain spatially

localised. The optical response is dominated by dielectric-like scattering. As the density increases beyond electrical percolation, extended conductive pathways emerge, yet optical transport remains limited by incomplete electromagnetic coupling between nanowires. When approaching the higher optical percolation threshold identified in our work ($amd_{\text{c,opt}}$), the interwire spacing becomes sufficiently small to enable strong near-field coupling and plasmonic hybridization, leading to the formation of delocalized collective modes across the network. This gives rise to an effective medium with metallic optical properties, consistent with the observed Hagen–Rubens behaviour.⁴⁹

The second possible interpretation draws from the framework of localization physics where increasing connectivity and coupling can drive a crossover from Anderson-type localised states towards delocalized ones⁵⁰ while enhanced carrier density and screening may evoke a Mott-like transition. In parallel, nanoplasmonic effects—particularly the emergence of coupled plasmon modes in dense networks—likely play a central role in shaping the infrared emissivity. Further theoretical discussion combining percolation theory, electrodynamics, and quantum transport will be essential to establish a unified description.

4. Conclusions

Metallic nanowire networks combine excellent intrinsic metal conductivity with a percolation-controlled architecture. Understanding and engineering their percolative nature—*via* control of nanowire dimension, junction chemistry and network topology, and *via* modelling that captures junction heterogeneity and bottlenecks—is the key route to improving their physical properties and reliability for the next generation of flexible and transparent devices. Our results show that, in addition to the well-known electrical percolation, there is also an optical percolation where the angular emissivity changes from dielectric to metallic behaviour. These two percolations occur at different critical network densities irrespective of nanowire diameter. The discovered percolative behaviour of multiple physical properties for just one material phase is what we call dual percolation. It must not be confused with the previously known double percolation of one property in multiple phases. We establish qualitatively that the optical percolation is related to a critical network gap size and determined that the corresponding gap diameter is much smaller than the wavelength of measured infrared radiation. This observation enables the fabrication of low-emissivity coatings with designed angular emissivity profile and opens a route to improved physical understanding of percolative networks. In addition, our work proves the applicability of the Hagen–Rubens relation for normal emissivity as a function of sheet resistance. Even though it was derived only for homogeneous thin metal films this dependence could also be applied in a generalised form to metallic nanowires exceeding a critical network density. All critical densities can be very well approximated as multiples of the simulated electrical percolation density with a ratio of



1:3.7:5.9 for electrical percolation, minimal Hagen–Rubens density, and optical percolation, respectively. Such ratio was found independent of the diameter of the silver nanowire, which ranged from 58 to 112 nm. Moreover, since the equivalent circular diameter (*ECD*) is much smaller compared to AgNW lengths, we anticipate that the observations of the dual percolation should remain valid when changing AgNW lengths (at least when the latter is larger than several micrometres). One of the prospects of this research work would be to investigate, through the same experimental tools, other MNW such as CuNW, Cu@Ni nanowires,⁵¹ or even coated AgNW with a thin layer of metal oxide. Such a study will assess the potential generalisation of the observations described in this article to other types of conductive nanowires including metallic ones or heavily doped semiconductors. The original observations reported in the present article provide new insights into the optical behaviour of MNW networks and offer valuable guidelines for optimizing their integration into industrial devices as well as new routes to understanding the macroscopic emissivity of microscopically inhomogeneous nanomaterials.

Author contributions

B. Zheng: conceptualisation, data analysis, formal analysis, investigation, methodology, visualisation, writing – original draft, writing – review & editing; S. Schumacher: data analysis, formal analysis, investigation, visualisation, writing – original draft, writing – review & editing; D. Muñoz-Rojas: supervision, writing – review & editing; J.-P. Simonato: supervision, writing – review & editing; D. Bellet: conceptualisation, formal analysis, funding acquisition, methodology, project administration, supervision, writing – original draft, writing – review & editing.

Conflicts of interest

There are no conflicts to declare.

Data availability

Data for this article are available on Zenodo at <https://doi.org/10.5281/zenodo.17799949>.

Supplementary information (SI) is available. See DOI: <https://doi.org/10.1039/d5mh02328a>.

Acknowledgements

B. Zheng acknowledges the financial support from the China Scholarship Council for his doctoral research grant. S. Schumacher acknowledges financial support from the European Union's Horizon Europe research and innovation programme under the Marie Skłodowska-Curie grant agreement No 101168616. Electron microscopy was performed at the CMTC characterisation platform of Grenoble INP, supported by the Centre of Excellence of Multifunctional Architected Materials “CEMAM” n° ANR-10-LABX-44-01 funded by the French

“Investments for the Future” program. The authors would like to warmly thank Laetitia Bardet, Amaury Baret and Ngoc Duy Nguyen for fruitful discussions.

References

- 1 Y. Ding, S. Xiong, L. Sun, Y. Wang, Y. Zhou, Y. Li, J. Peng, K. Fukuda, T. Someya, R. Liu and X. Zhang, Metal nanowire-based transparent electrode for flexible and stretchable optoelectronic devices, *Chem. Soc. Rev.*, 2024, **53**, 7784–7827, DOI: [10.1039/d4cs00080c](https://doi.org/10.1039/d4cs00080c).
- 2 S. Maurya, L. Labeyrie, K. Zimny, M. D. M. Rodriguez-Robles, B. Zheng, S. Schumacher, D. Muñoz-Rojas, D. Bellet and M. Tréguer-Delapierre, Recent advances in metallic nanowire based transparent electrodes: from chemistry of metallic nanowires to physics behind the conducting networks, *Adv. Phys. X*, 2025, **10**(1), 2573818, DOI: [10.1080/23746149.2025.2573818](https://doi.org/10.1080/23746149.2025.2573818).
- 3 J. J. Patil, W. H. Chae, A. Trebach, K. Carter, E. Lee, T. Sannicola and J. C. Grossman, Failing Forward: Stability of Transparent Electrodes Based on Metal Nanowire Networks, *Adv. Mater.*, 2021, **33**(5), 2004356, DOI: [10.1002/adma.202004356](https://doi.org/10.1002/adma.202004356).
- 4 T. Sannicola, M. Lagrange, A. Cabos, C. Celle, J.-P. Simonato and D. Bellet, Metallic Nanowire-Based Transparent Electrodes for Next Generation Flexible Devices: a Review, *Small*, 2016, **12**(44), 6052–6075, DOI: [10.1002/sml.201602581](https://doi.org/10.1002/sml.201602581).
- 5 V. H. Nguyen, D. T. Papanastasiou, J. Resende, L. Bardet, T. Sannicola, C. Jiménez, D. Muñoz-Rojas, N. D. Nguyen and D. Bellet, Advances in Flexible Metallic Transparent Electrodes, *Small*, 2022, **18**(19), 2106006, DOI: [10.1002/sml.202106006](https://doi.org/10.1002/sml.202106006).
- 6 D. T. Papanastasiou, E. Carlos, D. Muñoz-Rojas, C. Jiménez, A. Pimentel, E. Fortunato, R. Martins and D. Bellet, Fully Solution-Based AgNW/AlO_x Nanocomposites for Stable Transparent Heaters, *ACS Appl. Electron. Mater.*, 2022, **4**(12), 5816–5824, DOI: [10.1021/acsaem.2c01007](https://doi.org/10.1021/acsaem.2c01007).
- 7 S. Hanauer, C. Celle, C. Crivello, H. Szabolics, D. Muñoz-Rojas, D. Bellet and J.-P. Simonato, Transparent and Mechanically Resistant Silver-Nanowire-Based Low-Emissivity Coatings, *ACS Appl. Mater. Interfaces*, 2021, **13**(18), 21971–21978, DOI: [10.1021/acsaami.1c02689](https://doi.org/10.1021/acsaami.1c02689).
- 8 D. Toybou, C. Celle, C. Aude-Garcia, T. Rabilloud and J.-P. Simonato, A toxicology-informed, safer by design approach for the fabrication of transparent electrodes based on silver nanowires, *Environ. Sci.: Nano*, 2019, **6**(2), 684–694, DOI: [10.1039/c8en00890f](https://doi.org/10.1039/c8en00890f).
- 9 C. Gabbett, A. G. Kelly, E. Coleman, L. Doolan, T. Carey, K. Synnatschke, S. Liu, A. Dawson, D. O'Suilleabhain, J. Munuera, E. Caffrey, J. B. Boland, Z. Sofer, G. Ghosh, S. Kinge, L. D. A. Siebbeles, N. Yadav, J. K. Vij, M. A. Aslam, A. Matkovic and J. N. Coleman, Understanding how junction resistances impact the conduction mechanism in nanonetworks, *Nat. Commun.*, 2024, **15**(1), 4517, DOI: [10.1038/s41467-024-48614-5](https://doi.org/10.1038/s41467-024-48614-5).



- 10 E. Coleman, A. Kelly, C. Gabbett, L. Doolan, S. Liu, N. Yadav, J. K. Vij and J. N. Coleman, Extracting the Temperature Dependence of Both Nanowire Resistivity and Junction Resistance from Electrical Measurements on Printed Silver Nanowire Networks, *ACS Appl. Electron. Mater.*, 2025, 7(2), 806–815, DOI: [10.1021/acsaelm.4c01965](https://doi.org/10.1021/acsaelm.4c01965).
- 11 L. Bardet, D. T. Papanastasiou, C. Crivello, M. Akbari, J. Resende, A. Sekkat, C. Sanchez-Velasquez, L. Rapenne, C. Jiménez, D. Muñoz-Rojas, A. Denneulin and D. Bellet, Silver Nanowire Networks: Ways to Enhance Their Physical Properties and Stability, *Nanomaterials*, 2021, 11(11), 2785, DOI: [10.3390/nano11112785](https://doi.org/10.3390/nano11112785).
- 12 Y. Chernukha, L. Bardet, M. Berthe, T. Lerond, J.-P. Mazellier, L. Gangloff, A. Denneulin, P. Diener and D. Bellet, *In Situ* Multiscale Investigation of Capillary-Force-Induced Cold-Welding of Silver Nanowire NetworksClick, *ACS Omega*, 2025, 10(46), 55716–55724, DOI: [10.1021/acsomega.5c07063](https://doi.org/10.1021/acsomega.5c07063).
- 13 D. P. Langley, M. Lagrange, N. D. Nguyen and D. Bellet, Percolation in networks of 1-dimensional objects: comparison between Monte Carlo simulations and experimental observations, *Nanoscale Horiz.*, 2018, 3(5), 545–550, DOI: [10.1039/c8nh00066b](https://doi.org/10.1039/c8nh00066b).
- 14 M. Lagrange, D. P. Langley, G. Giusti, C. Jiménez, Y. Bréchet and D. Bellet, Optimization of silver nanowire-based transparent electrodes: effects of density, size and thermal annealing, *Nanoscale*, 2015, 7(41), 17410–17423, DOI: [10.1039/c5nr04084a](https://doi.org/10.1039/c5nr04084a).
- 15 W. Li, X. Zhao, G. Xie, X. Luo, X. Cheng and Y. Su, Programmable high-performance ternary piezoelectric nanogenerators by synergizing reinforcement effect and percolation effect, *Mater. Today Chem.*, 2025, 48, 102955, DOI: [10.1016/j.mtchem.2025.102955](https://doi.org/10.1016/j.mtchem.2025.102955).
- 16 T. Sanniccolo, D. Muñoz-Rojas, N. D. Nguyen, S. Moreau, C. Celle, J.-P. Simonato, Y. Bréchet and D. Bellet, Direct Imaging of the Onset of Electrical Conduction in Silver Nanowire Networks by Infrared Thermography: Evidence of Geometrical Quantized Percolation, *Nano Lett.*, 2016, 16(11), 7046–7053, DOI: [10.1021/acs.nanolett.6b03270](https://doi.org/10.1021/acs.nanolett.6b03270).
- 17 J. Wu, W. Wang, X. Chen and N. Li, Double percolation and segregated structures formed in polymer alloy with excellent electrical conductivity, *Polym. Compos.*, 2021, 42(2), 693–700, DOI: [10.1002/pc.25858](https://doi.org/10.1002/pc.25858).
- 18 I. Y. Forero-Sandoval, A. P. Franco-Bacca, F. Cervantes-Álvarez, C. L. Gómez-Heredia, J. A. Ramírez-Rincón, J. Ordóñez-Miranda and J. J. Alvarado-Gil, Electrical and thermal percolation in two-phase materials: A perspective, *J. Appl. Phys.*, 2022, 131(23), 230901, DOI: [10.1063/5.0091291](https://doi.org/10.1063/5.0091291).
- 19 Y. Liu, H. He, G. Tian, Y. Wang, J. Gao, C. Wang, L. Xu and H. Zhang, Morphology evolution to form double percolation polylactide/polycaprolactone/MWCNTs nanocomposites with ultralow percolation threshold and excellent EMI shielding, *Compos. Sci. Technol.*, 2021, 214, 108956, DOI: [10.1016/j.compscitech.2021.108956](https://doi.org/10.1016/j.compscitech.2021.108956).
- 20 K. H. Kim, J.-U. Jang, G. Y. Yoo, S. H. Kim, M. J. Oh and S. Y. Kim, Enhanced Electrical and Thermal Conductivities of Polymer Composites with a Segregated Network of Graphene Nanoplatelets, *Materials*, 2023, 16(15), 5329, DOI: [10.3390/ma16155329](https://doi.org/10.3390/ma16155329).
- 21 N.-A. Masarra, J.-C. Quantin, M. Batistella, R. El Hage, M. F. Pucci and J.-M. Lopez-Cuesta, Influence of Polymer Processing on the Double Electrical Percolation Threshold in PLA/PCL/GNP Nanocomposites, *Sensors*, 2022, 22(23), 9231, DOI: [10.3390/s22239231](https://doi.org/10.3390/s22239231).
- 22 T. Kajornprai, R. Jarapanyacheep, J. Saikaeo, S. Pojprapai, K. Jarukumjorn and T. Trongsatitkul, Double Percolation of Poly(lactic acid)/Low-Density Polyethylene/Carbon Nanotube (PLA/LDPE/CNT) Composites for Force-Sensor Application: Impact of Preferential Localization and Mixing Sequence, *Polymers*, 2024, 16(13), 1906, DOI: [10.3390/polym16131906](https://doi.org/10.3390/polym16131906).
- 23 D. Bellet, M. Lagrange, T. Sanniccolo, S. Aghazadehchors, V. H. Nguyen, D. P. Langley, D. Muñoz-Rojas, C. Jiménez, Y. Bréchet and N. D. Nguyen, Transparent Electrodes Based on Silver Nanowire Networks: From Physical Considerations towards Device Integration, *Materials*, 2017, 10(6), 570, DOI: [10.3390/ma10060570](https://doi.org/10.3390/ma10060570).
- 24 J. Lee and J. Nam, Percolation threshold of curved linear objects, *Phys. Rev. E*, 2021, 103(1), 012126, DOI: [10.1103/PhysRevE.103.012126](https://doi.org/10.1103/PhysRevE.103.012126).
- 25 J. I. Diaz Schneider, C. P. Quinteros, P. Levy and E. D. Martínez, Two-Junction Model in Different Percolation Regimes of Silver Nanowires Networks, *Adv. Funct. Mater.*, 2024, 34(52), 2410766, DOI: [10.1002/adfm.202410766](https://doi.org/10.1002/adfm.202410766).
- 26 C. Forró, L. Demkó, S. Weydert, J. Vörös and K. Tybrandt, Predictive Model for the Electrical Transport within Nanowire Networks, *ACS Nano*, 2018, 12(11), 11080–11087, DOI: [10.1021/acsnano.8b05406](https://doi.org/10.1021/acsnano.8b05406).
- 27 T. Araki, J. Jiu, M. Nogi, H. Koga, S. Nagao, T. Sugahara and K. Suganuma, Low haze transparent electrodes and highly conducting air dried films with ultra-long silver nanowires synthesized by one-step polyol method, *Nano Res.*, 2014, 7(2), 236–245, DOI: [10.1007/s12274-013-0391-x](https://doi.org/10.1007/s12274-013-0391-x).
- 28 K. Chen, B. Zhao, L. Wu, T. Hu, Y. Xiang, T. Chen and G. Pei, Silver nanowire networks on textured silicon as low-emissivity coatings for photovoltaic/thermal applications, *Sol. Energy*, 2024, 267, 112253, DOI: [10.1016/j.solener.2023.112253](https://doi.org/10.1016/j.solener.2023.112253).
- 29 A. Baret, A. Khan, A. Rougier, D. Bellet and N. D. Nguyen, Low-emissivity fine-tuning of efficient VO₂-based thermochromic stacks with silver nanowire networks, *RSC Appl. Interfaces*, 2025, 2(1), 94–103, DOI: [10.1039/d4lf00234b](https://doi.org/10.1039/d4lf00234b).
- 30 M. Dressel and G. Grüner, *Electrodynamics of Solids: Optical Properties of Electrons in Matter*, Cambridge University Press, Cambridge, New York, 2002.
- 31 R. E. Hummel, *Electronic Properties of Materials*, Springer, Berlin, Heidelberg, 3rd edn, 2001.
- 32 B. Guo, Y. Wang, C. Cao, Z. Qu, J. Song, S. Li, J. Gao, P. Song, G. Zhang, Y. Shi and L. Tang, Large-Scale, Mechanically Robust, Solvent-Resistant, and Antioxidant MXene-Based Composites for Reliable Long-Term Infrared Stealth, *Adv. Sci.*, 2024, 11(17), 2309392, DOI: [10.1002/advs.202309392](https://doi.org/10.1002/advs.202309392).



- 33 P. Schmitt, N. Felde, T. Döhring, M. Stollenwerk, I. Uschmann, K. Hanemann, M. Siegler, G. Klemm, N. Gratzke, A. Tünnermann, S. Schwinde, S. Schröder and A. Szeghalmi, Optical, structural, and functional properties of highly reflective and stable iridium mirror coatings for infrared applications, *Opt. Mater. Express*, 2022, **12**(2), 545–559, DOI: [10.1364/ome.447306](https://doi.org/10.1364/ome.447306).
- 34 T. Brandt, M. Hövel, B. Gompf and M. Dressel, Temperature- and frequency-dependent optical properties of ultrathin Au films, *Phys. Rev. B: Condens. Matter Mater. Phys.*, 2008, **78**(20), 205409, DOI: [10.1103/PhysRevB.78.205409](https://doi.org/10.1103/PhysRevB.78.205409).
- 35 M. Born, E. Wolf, A. B. Bhatia, P. C. Clemmow, D. Gabor, A. R. Stokes, A. M. Taylor, P. A. Wayman and W. L. Wilcock, *Principles of Optics: Electromagnetic Theory of Propagation, Interference and Diffraction of Light*, Cambridge University Press, Cambridge, New York, 7th edn, 1999.
- 36 A. Seifert, About the Meaning of the Hagen–Rubens Relation to Radiation Thermometry, *Metrology in the 3rd Millennium*, XVII IMEKO World Congress, 2003, pp. 1695–1698.
- 37 M. F. Modest and S. Mazumder: *Radiative heat transfer*, Academic Press, London, 4th edn, 2022.
- 38 D. T. Papanastasiou, Investigation of silver nanowire networks: physical properties, stability and integration into devices PhD thesis, Univ. Grenoble Alpes, 2020, DOI: [10.70675/392da118zef59z454dzac54zd242a99e87cb](https://doi.org/10.70675/392da118zef59z454dzac54zd242a99e87cb).
- 39 P. J. Yunker, T. Still, M. A. Lohr and A. G. Yodh, Suppression of the coffee-ring effect by shape-dependent capillary interactions, *Nature*, 2011, **476**, 308–311, DOI: [10.1038/nature10344](https://doi.org/10.1038/nature10344).
- 40 C. Steger, An unbiased detector of curvilinear structures, *IEEE Trans. Pattern Anal. Mach. Intell.*, 1998, **20**, 113–125, DOI: [10.1109/34.659930](https://doi.org/10.1109/34.659930).
- 41 T. Wagner, M. Hiner and X. Raynaud, Ridge Detection 1.4.0, Zenodo, 2017, DOI: [10.5281/zenodo.845874](https://doi.org/10.5281/zenodo.845874).
- 42 J. Schindelin, I. Arganda-Carreras, E. Frise, V. Kaynig, M. Longair, T. Pietzsch, S. Preibisch, C. Rueden, S. Saalfeld, B. Schmid, J.-Y. Tinevez, D. J. White, V. Hartenstein, K. Eliceiri, P. Tomancak and A. Cardona, Fiji: an open-source platform for biological image analysis, *Nat. Methods*, 2012, **9**(7), 676–682, DOI: [10.1038/nmeth.2019](https://doi.org/10.1038/nmeth.2019).
- 43 O. Riou, P.-O. Logerais and J.-F. Durastanti, Quantitative study of the temperature dependence of normal LWIR apparent emissivity, *Infrared Phys. Technol.*, 2013, **60**, 244–250, DOI: [10.1016/j.infrared.2013.05.012](https://doi.org/10.1016/j.infrared.2013.05.012).
- 44 E. Schmidt and E. Eckert, Über die Richtungsverteilung der Wärmestrahlung von Oberflächen, *Forsch. Ingenieurw.*, 1935, **6**(4), 175–183, DOI: [10.1007/bf02578830](https://doi.org/10.1007/bf02578830).
- 45 E. Hecht, *Optics*, Addison-Wesley, San Francisco, 4th edn, 2010.
- 46 J. Li and S.-L. Zhang, Finite-size scaling in stick percolation, *Phys. Rev. E: Stat., Nonlinear, Soft Matter Phys.*, 2009, **80**(4), 040104, DOI: [10.1103/PhysRevE.80.040104](https://doi.org/10.1103/PhysRevE.80.040104).
- 47 M. Iskander and L. Li, *Dynamic Image Analysis of Granular Materials: Particle Granulometry for Geotechnical, Material, and Geological Applications*, Springer, Cham, 1st edn, 2024.
- 48 U. Schnepf, M. A. L. von Moers-Meißner and F. Brümmer, A practical primer for image-based particle measurements in microplastic research, *Microplast. Nanoplast.*, 2023, **3**(1), 16, DOI: [10.1186/s43591-023-00064-4](https://doi.org/10.1186/s43591-023-00064-4).
- 49 V. E. Babicheva, Y.-J. Lu, A. Shalin and D. Late, Introduction to Advances in nanophotonics, plasmonics, and nano-optic, *Nanoscale Adv.*, 2025, **7**(21), 6674–6676, DOI: [10.1039/d5na90067k](https://doi.org/10.1039/d5na90067k).
- 50 Z. Qi, Y. Zhang, M. Qin, H. Weng and K. Jiang, Anderson Localization: A Density Matrix Approach, *Phys. Rev. X*, 2026, **16**(1), 011043, DOI: [10.1103/y5kd-7prs](https://doi.org/10.1103/y5kd-7prs).
- 51 A. Križan, L. Bardet, K. Zimny, M. Romanus, M. Berthe, C. Labrugère-Saroste, D. Bellet and M. Tréguer-Delapierre, Oxidation-Resistant Cu-Based Nanowire Transparent Electrodes Activated by an Exothermic Reduction Reaction, *ACS Nano*, 2024, **18**(51), 34902–34911, DOI: [10.1021/acsnano.4c12698](https://doi.org/10.1021/acsnano.4c12698).

